

## $F_2$ challenging DGLAP

D. Haidt

DESY, Notkestr. 85, 22607 Hamburg, Germany

Received: 31 October 2003 /

Published online: 26 May 2004 – © Springer-Verlag / Società Italiana di Fisica 2004

**Abstract.** The low- $x$  data of the structure function  $F_2$  measured by the collaborations H1 and ZEUS are compared with the prediction of the DGLAP equations. A new method of comparing data and theory is presented. The systematic and quantitative analysis shows that the predicted  $1/x$  behavior deviates increasingly from the observed one as  $x$  decreases below  $10^{-3}$ .

### 1 Introduction

Lepton–nucleon experiments have paved the way towards the standard model with the observation of the proton substructure and the observation of weak neutral currents. Together with the ideas on gauge theories based on non-abelian algebras and renormalizability a new framework for electroweak and strong interactions has been set up. A worldwide long term program was initiated.

The intermediate  $\gamma$  in  $e$ –nucleon and the intermediate  $W$  in  $\nu$ –nucleon scattering probe the same internal structure of the nucleon. The quark–parton model provided a simple interpretation of lepton–nucleon scattering, like for instance the structure function  $F_2$  as a manifestation of the fractional momentum distribution of quarks and antiquarks in the nucleon. The precise measurement of the momentum sum rule in the Gargamelle  $\nu$  experiment [1] resulted in  $0.50 \pm 0.03$  rather than 1. This surprising result indicated that quarks and antiquarks by far do not make up the momentum of the nucleon, and another novel type of constituents, not visible to the  $W$ , must be present. They were attributed to the gluons as carriers of the strong force in the new microscopic theory of strong interactions, QCD [2]. The apparently free behavior of the partons observed in deep inelastic lepton–nucleon scattering found its explanation in the property of the strong force to decrease at short distances. The immediate consequence was that the nucleon structure functions cannot be functions of the Bjorkén scaling variable  $x$  alone, but must depend on both kinematic variables characterizing deep inelastic scattering, namely  $x$  and  $Q^2$ , where  $Q^2$  is the 4-momentum transfer squared from the lepton to the hadron system.

An impressive series of leptoproduction experiments of increasing precision was carried out. The differential cross section depends upon the three structure functions  $F_2$ ,  $F_L$  and  $xF_3$ .  $\nu$ ,  $\bar{\nu}$  experiments were distinguished by measuring in addition to  $F_2$  also  $xF_3$ . The deep inelastic scattering experiments constituted a solid testing ground for QCD. In the kinematic regime, where  $Q^2$  is sufficiently large, typ-

ically larger than  $1 \text{ GeV}^2$ , the strong interaction coupling constant  $\alpha_s(Q^2)$  is small and a perturbative treatment is possible. The DGLAP evolution equations [3, 4] offered an elegant way to test perturbative QCD in deep inelastic scattering experiments through the investigation of the deviation from scaling. Given the structure functions or the parton distribution functions as a function of  $x$  for a chosen starting value,  $Q_{st}^2$ , QCD predicts the  $Q^2$  evolution. The comparison between theory and experiment always involved a double aspect: the determination of the parton distribution functions, which cannot be predicted, and the properties of the theory to be tested.

The tests performed in the 70's and 80's were a great success and established the validity of the DGLAP equations in the  $(Q^2, 1/x)$ -phase space delimited to a triangular area determined by the size of the available beam energy, in practice reaching out for  $Q^2$  to a few  $100 \text{ GeV}^2$  and for  $x$  down to slightly below  $10^{-2}$ . In comparing and interpreting the wealth of measurements, there remained nevertheless a serious concern related to the arbitrariness in distinguishing the perturbative from the non-perturbative regime and to the correlations caused by the unknown gluon distribution function. As a matter of fact, the  $Q^2$  evolution of the structure function  $xF_3$  measured in  $\nu$ ,  $\bar{\nu}$  experiments tests QCD independently of assumptions about the gluon; however, its statistical significance was much less than the precise  $F_2$  measurements, which strongly depend upon assumptions about the gluon distribution function.

A new era of QCD tests started with the running of the  $ep$ -collider HERA 1992, which extended the phase space by two orders of magnitude in  $Q^2$  and in  $x$ . The first data in the low- $x$  region revealed a huge rise and thereby a new feature in the phenomenology of  $F_2$ . The subsequent detailed measurements by H1 [5] and ZEUS [6] offered new tests of QCD. They were performed by the experimental groups themselves as well as by various groups of theoreticians. Recent global fits by MRST [7], CTEQ [8], GRV [9] including the HERA data on  $F_2$  resulted in good fits supporting thus the validity of the DGLAP evolution in the

valence region up to  $Q^2$  of order  $10^4 \text{ GeV}^2$  and in the sea region, down to  $x = 10^{-5}$ , up to the phase space limit. The successful extension of the fits up to the largest  $Q^2$  values was expected. That the fits would still work at low  $x$  was rather a surprise, as many were prepared to witness a failure of the perturbative approach, where terms with  $\log 1/x$  should get numerically more and more prominent.

It is the purpose of this study to focus on the low- $x$  regime of the  $(Q^2, 1/x)$ -phase space available in the HERA experiments, to investigate there in detail the rôle of the  $1/x$  terms in the DGLAP kernels and to show that for  $x$  below  $10^{-3}$  a discrepancy between theory and experiment develops.

## 1.1 Outline

Section 2 recalls some phenomenological aspects of  $F_2^{ep}$  reformulated in terms of a new variable  $q$  replacing  $\ln Q^2$ . A new method of comparing data and theory is presented in Sect. 4, which makes use of  $F_2$ , and of its first and second derivative in  $Q^2$ . The next section describes the decomposition of  $F_2^{ep}$  into a singlet and a non-singlet part. Section 5 deals with the DGLAP equations formulated in terms of  $q$  and illustrates their effect when applied to a valence-like and a sea-like distribution separately for leading and next-to-leading order. After these preparations the main step is taken in Sect. 7 with the evaluation of the curvature of the singlet part and  $F_2^{ep}$  itself. The last section concludes with the comparison of data and theory.

## 2 Phenomenology of $F_2$

The investigation of the  $Q^2$  behavior of the early low- $x$   $F_2$  data measured by the HERA collaborations H1 and ZEUS suggested an approximate scaling behavior [10,11] of the form  $F_2 \sim \log Q^2/Q_0^2$  with  $Q_0^2 \approx 0.5 \text{ GeV}^2$ . With the advent of further measurements extending to  $Q^2 < 1 \text{ GeV}^2$  it was desirable to have, instead of the usual  $\ln Q^2$ , a quantity which allows one to examine the  $Q^2$  dependence of the  $F_2$  data in the neighborhood of 0. This is achieved [12] with the quantity<sup>1</sup>

$$q = \log(1 + Q^2/Q_0^2), \quad (1)$$

where  $Q_0^2$  is a constant set to  $0.5 \text{ GeV}^2$ . The new quantity  $q$  is mathematically equivalent to the traditional  $\ln Q^2$ , but has the feature to run from 0 to  $\infty$ . For  $Q^2 \gg Q_0^2$   $q$  is equivalent to  $\ln Q^2$ , while otherwise it approaches  $Q^2$ . Figure 1 illustrates the  $F_2$  measurements by H1 [5] and ZEUS [6] as a function of  $q$  for a  $x$ -bin centered at  $x = 10^{-4}$ . The structure function is within experimental uncertainties proportional to  $q$  over the full measured range corresponding to  $Q^2$  from about  $0.3$  until  $6.7 \text{ GeV}^2$ , i.e. near the HERA phase space limit. When the  $F_2$  points are extrapolated towards  $Q^2 = 0$  by a linear fit, a value for  $F_2$  consistent with 0 comes out in agreement with the conservation of the electromagnetic current.

<sup>1</sup>  $\log$  is taken to base 10.

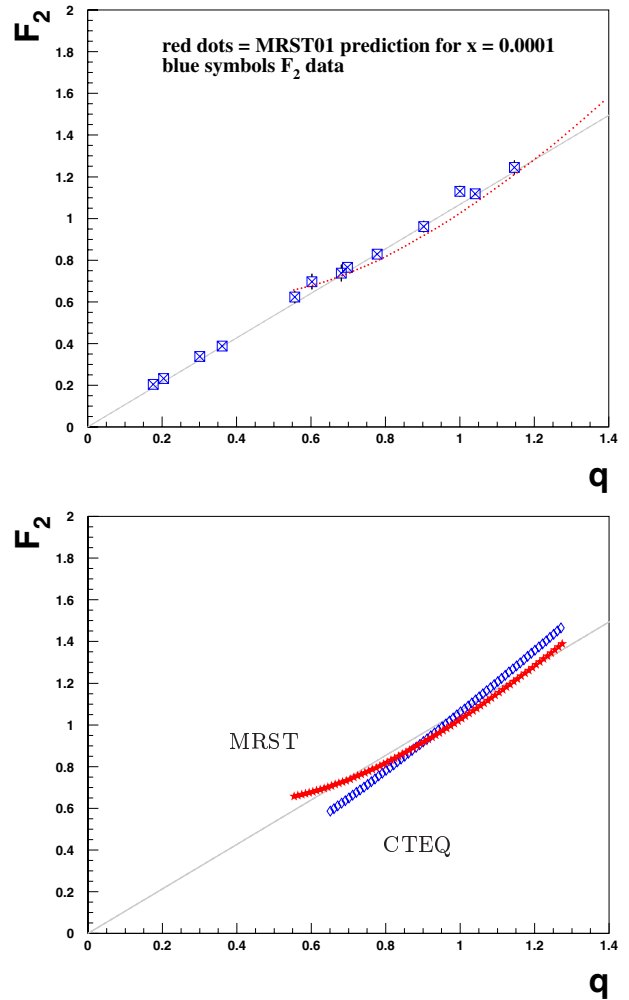


**Fig. 1.** The above figure shows the  $q$  dependence of the  $F_2$  data for  $x$ -bin centered at  $x = 10^{-4}$ ; the dotted line is the prediction of the MRST01 parametrization. In the figure below predictions of the MRST01 and the CTEQ6 parametrization are compared for  $x = 10^{-4}$

Figure 1 shows also by the dotted line the prediction of the MRST parametrization [7] for  $x = 10^{-4}$ , which is the result of their global fit. The fit is based on the  $x$  dependence of the parton distributions a priori assumed at the starting scale  $Q_{\text{st}}^2 = 1.25 \text{ GeV}^2$ , i.e.  $q_{\text{st}} = 0.54$ , and then evolved in  $Q^2$  using the DGLAP evolution equations (see (4)). The free parameters of the initial parton distributions are varied in an iterative procedure until the overall data and prediction yield a minimal  $\chi^2$ . The comparison of the dotted line with the measured points illustrates that the global fit in this particular  $x$ -bin is a best fit, though not a good fit. In fact, there seems to be an indication for a difference in shape. This suggests the size of the second derivative of  $F_2$  with respect to  $q$  to serve as a test quantity in examining the validity of DGLAP in the deep sea.

The data of  $F_2$  in the deep sea are well described by a second order polynomial in  $q$ :

$$F_2(x, q) = a_0(x) + a_1(x) \cdot q + a_2(x) \cdot q^2,$$

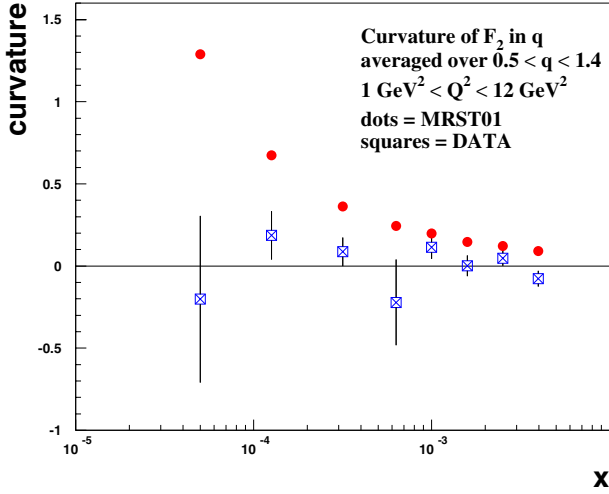


**Fig. 2.** Curvature of  $F_2$  averaged over the interval  $0.5 < q < 1.4$  for various fixed  $x$ -bins; the data points (squares) are compared with the MRST prediction

where  $a_0(x)$  and  $a_2(x)$  are approximately 0, as seen for example in Fig. 1. This form remains valid even in the valence region as long as  $q$  is restricted to the interval  $(0.5, 2)$ . The curvature term  $a_2(x)$  is obtained as the second derivative of  $F_2$  with respect to  $q$ , namely  $\partial_q^2 F_2(x, q) = 2 a_2(x)$ .

Figure 2 shows the curvature term  $a_2(x)$  for the data at various fixed  $x$ -bins in comparison with the prediction of MRST. The lower limit in  $q$  is set to the starting scale for the DGLAP evolution in the MRST fit. The upper limit is chosen as small as possible, such that there are still enough measurements to determine the curvature. This requirement led to  $Q^2 < 12 \text{ GeV}^2$  or  $q < 1.4$ , unless the HERA phase space limit is smaller. The experimental points are shown by the crosses, the MRST points by the dots. The MRST points are obtained applying the same procedure, but replacing the measured  $F_2$  values by the corresponding values predicted by MRST. It should be noted that the average value of  $q$  decreases with decreasing  $x$  due to the more and more restricted phase space. The data are consistent with being flat in  $q$ , while the MRST prediction deviates the more the smaller  $x$  is.

### 3 Method of analysis

The traditional way of testing the linear system of coupled DGLAP equations (see (4)) consists in performing the  $Q^2$  evolution in the form of a global fit, as indicated above (c.f. Sect. 2). One single quantity, the overall  $\chi^2$ , holds simultaneously the information on the shape of the parton distribution functions and on the validity of the DGLAP equations. A good fit means merely a consistency check for QCD.

A curve can be characterized in two distinct ways: either by points over a finite size or infinitesimally by one point and derivatives at this point. The method proposed here and elaborated below relies on the latter characterization.

Instead of performing the evolution of the singlet over the range in  $q$ , where measurements exist, the singlet is studied locally in  $q$  and the information about the  $q$  behavior is accounted for by considering the higher order derivatives with respect to  $q$ .

For all subsequent numerical calculations  $q$  is chosen to be 1, corresponding to  $Q^2 = 4.5 \text{ GeV}^2$ . This value is big enough to justify the use of perturbative QCD and small enough to access the HERA  $F_2$  measurements down to  $x = 10^{-5}$ , leaving two orders of magnitude in  $x$  for probing the low- $x$  properties of the DGLAP kernels.

Given as input distributions the singlet  $Q^+(x, 1)$  and its derivative  $\partial_q Q^+(x, 1)$ , the gluon distribution function  $G(x, 1)$  is derived from the first of the coupled DGLAP equations, as elaborated below in Sect. 7. In the next step the second derivative  $\partial_q^2 Q^+(x, 1)$  is calculated. There the unknown derivative  $\partial_q G(x, 1)$  emerges. The second of the coupled DGLAP equations provides precisely this term. The quantity  $\partial_q^2 Q^+(x, 1)$  is calculated in the deep sea and after relating it to  $\partial_q^2 F_2(x, 1)$  is compared with the experimentally determined curvature. This completes the local test of the validity of the DGLAP equations.

### 4 Decomposition of $F_2^{ep}$

The  $Q^2$  evolution of the structure function  $F_2$  in  $ep$  scattering proceeds differently for the singlet and the non-singlet part. The QCD expression for  $F_2^{ep}$  is given in terms of the quark ( $q_i(x, Q^2)$ ) and antiquark ( $\bar{q}_i(x, Q^2)$ ) density functions for each flavor  $i$  and the gluon function  $g(x, Q^2)$ :

$$F_2^{ep} = C_F \otimes N + \epsilon (C_F \otimes Q^+ + C_G \otimes G). \quad (2)$$

This is the standard decomposition (see e.g. [13]). The meaning of the variables is as follows.

- Singlet:  $Q^+ = \sum_i^f x(q_i + \bar{q}_i)$  with  $f$  the number of active flavors.
- QED coupling constants:  $e_i^2$  for flavor  $i$ .
- $\epsilon = \frac{1}{f} \sum_i^f e_i^2$ .
- Non-singlet:  $N = \sum_i^f e_i^2 \left( x(q_i + \bar{q}_i) - \frac{1}{f} Q^+ \right)$ .
- Gluon:  $G = xg$ .
- Coefficient functions  $C_F$  and  $C_G$ :  $C_F$  has a leading  $\delta$  function and an  $\mathcal{O}(\alpha_s/2\pi)$  contribution, while  $C_G$  is directly of order to  $\mathcal{O}(\alpha_s/2\pi)$ .

The  $\overline{\text{MS}}$  scheme is used and four massless quarks.  $F_2^{ep}$  is dominated by  $N + \epsilon Q^+$ , but receives subleading contributions from both the quarks and the gluon through the coefficient functions.

Detailed  $F_2^{ep}$  measurements are available from the two HERA collaborations H1 [5] and ZEUS [6]. The collaborations have provided in their publications careful analyses of systematic error sources. In their kinematic overlap region the data sets agree well, once the systematics is taken into account. Some of the correlated systematic sources affect not only the absolute values  $F_2$ , but also the derivative  $\partial_q F_2$ .

The structure function  $F_2^{ep}$  (see (2)) is dominated by  $\epsilon Q^+$  and receives contributions from the coefficient functions at  $\mathcal{O}(\alpha_s/2\pi)$  and from the non-singlet. For the actual calculations done below for  $q = 1$  it is then a good approximation to relate the  $x$  distributions of the singlet and its derivative to the well measured structure function, as follows:

$$\begin{aligned} Q^+(x, 1) &= \frac{1}{\epsilon} F_2^{\text{meas}}(x, 1), \\ \partial_q Q^+(x, 1) &= \frac{1}{\epsilon} \partial_q F_2^{\text{meas}}(x, 1). \end{aligned} \quad (3)$$

In the kinematic region of interest, the deep sea with  $x < 0.001$ , the non-singlet distribution contributes little to  $F_2$  and  $\partial_q F_2$ . Furthermore, the convolutions of  $Q^+$  and  $G$  with the coefficient functions only moderately modify the shape of the singlet distribution, both for the  $x$  and  $Q^2$  dependences. The small corrections implied by the identification given in (3) are considered in Sect. 8.

## 5 The DGLAP equations

From the parton density functions of the quarks  $q_f(x, Q^2)$ , and antiquarks  $\bar{q}_f(x, Q^2)$ , for the active flavors  $f$  and the gluon  $g(x, Q^2)$  one can form the following distributions:

$$\begin{aligned} \text{Valence : } Q^- &= \sum x(q_i - \bar{q}_i), \\ \text{Singlet : } Q^+ &= \sum x(q_i + \bar{q}_i), \\ \text{Gluon : } G &= xg. \end{aligned}$$

For the values of  $Q^2$  considered  $f = 4$  is assumed, and furthermore all quarks are taken to be massless.

The DGLAP integro-differential equations for the singlet and the gluon read in compact form

$$\partial_q \begin{pmatrix} Q^+ \\ G \end{pmatrix} = a(q) \begin{pmatrix} P_{qq} & P_{qg} \\ P_{gq} & P_{gg} \end{pmatrix} \otimes \begin{pmatrix} Q^+ \\ G \end{pmatrix}. \quad (4)$$

The equations are formulated in terms of the variable  $q$ , rather than the usual  $\ln Q^2$ . The variable transformation  $\ln Q^2 \rightarrow q = \log(1 + Q^2/Q_0^2)$  implies

$$dq = \frac{Q^2}{Q^2 + Q_0^2} \frac{1}{\ln 10} d \ln Q^2,$$

where the Jacobi factor  $Q^2/(Q^2 + Q_0^2)$  appears and the factor  $\ln 10$ , since the variable  $q$  is defined with log to base 10. The notation  $\partial_q$  is a shorthand for  $\partial/\partial q$ . Furthermore,

$$a(q) = \frac{\alpha_s(Q^2)}{2\pi} \frac{Q^2 + Q_0^2}{Q^2} \ln 10.$$

It is interesting to note that  $q \cdot a(q)$  has only a small  $Q^2$  dependence: it increases by 3% in going from 5 to 50 GeV<sup>2</sup> and decreases by 3% in going from 5 to 1 GeV<sup>2</sup>.

The kernels  $P_{ij}$  describe the splitting of the parton  $j \rightarrow i$ . They are used in next-to-leading order in the  $\overline{\text{MS}}$  scheme as published in [13]:

$$P(x, \alpha_s) = P^{\text{LO}}(x) + \frac{\alpha_s}{2\pi} P^{\text{NLO}}(x).$$

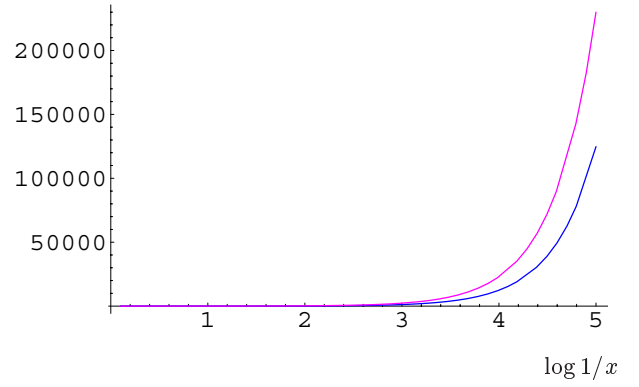


**Fig. 3.** The kernels  $P_{qg}$  and  $P_{gg}$  versus  $\log 1/x$ ; the upper curve refers to  $P_{gq}$ . The  $\log 1/x$  starts at 0.1 excluding the singular behavior of  $x$  near 1

The leading and next-to-leading kernels are by themselves functions of  $x$  alone. However, the full kernels receive a  $Q^2$  dependence indirectly through the  $Q^2$  dependence of the QCD coupling  $\alpha_s$ .

A characteristic feature of all four kernels consists in the fact that they contain in next-to-leading order terms proportional to  $1/x$ , the two kernels  $P_{qg}$  and  $P_{gg}$  even already at lowest order. Their presence provokes an almost explosive rise at values of  $x < 0.001$ , as illustrated in Fig. 3 for the off-diagonal kernels  $P_{qg}$  and  $P_{gq}$ . Their behavior becomes singular for  $x \rightarrow 1$  and is not shown. In the deep sea region the  $x$  behavior of  $P_{qg}$  and  $P_{gq}$  is similar; this leads in their ratio to a nearly  $x$  independent shape, as displayed in Fig. 4. The two diagonal kernels  $P_{qq}$  and  $P_{gg}$  include *distributions*, i.e. *plus* and  $\delta$  functions, and cannot be displayed directly. Instead, the properties of a kernel  $P$  can be studied by comparing a given distribution function  $f$  with the corresponding folded distribution function  $P \otimes f$ :

$$f(x) \rightarrow P \otimes f(x).$$

The convolution of a function  $f(x)$  with the kernel  $P(x)$  is defined by

$$P \otimes f(x) = \int_x^1 d\xi P(\xi) f\left(\frac{x}{\xi}\right).$$

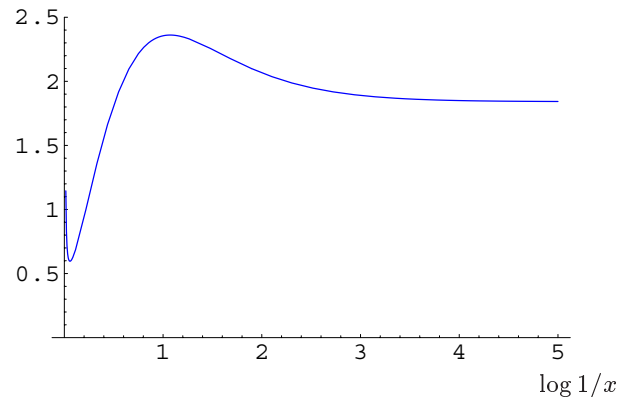


**Fig. 4.** The ratio  $P_{qg}/P_{gq}$  for  $0.00001 < x < 0.97$

The integral runs from  $x$  to 1, consequently the value of the folded distribution at  $\hat{x}$  involves the functional dependence of the input function from  $\hat{x}$  until 1. The graphical representation of the  $x$  dependence is conveniently given in terms of  $\log 1/x$ .

For illustration the convolution effect is demonstrated for two ad hoc, but typical functions, a *valence*-like distribution ( $f_{\text{val}}$ ) and *sea*-like distribution ( $f_{\text{sea}}$ ).

### 5.1 Study of $f_{\text{val}}(x) \rightarrow a(q) P(x, \alpha_s(q)) \otimes f_{\text{val}}(x)$

Figure 5 shows on top the *valence*-like distribution,

$$f_{\text{val}}(x) = 3.28 \sqrt{x}(1-x)^3,$$

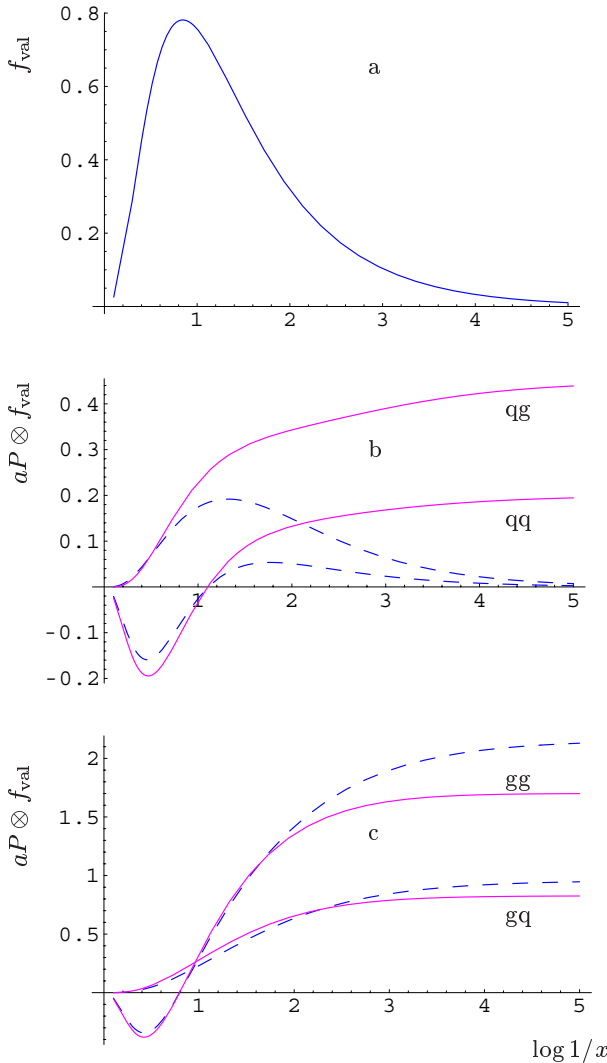


**Fig. 5.** **a** The valence-like distribution  $f_{\text{val}}(x)$  versus  $\log 1/x$ . **b**  $a(q) P_{qq} \otimes f_{\text{val}}$  and  $a(q) P_{gg} \otimes f_{\text{val}}$  for  $q = 1$  versus  $\log 1/x$ . **c**  $a(q) P_{gg} \otimes f_{\text{val}}$  and  $a(q) P_{gq} \otimes f_{\text{val}}$  for  $q = 1$  versus  $\log 1/x$ . The solid (dashed) curves show the convolution with the full (leading) order kernel marked with the appropriate indices. The curves resulting from the folding with the diagonal kernels  $P_{qq}$  and  $P_{gg}$  show the characteristic underswinger in the valence region

and below ((b) and (c)) for  $q = 1$  the distributions resulting from the folding with the four kernels. The factor 3.28 is chosen to make the integral over the corresponding density equal to 3. The diagonal kernels generate the characteristic shape, which causes the depletion of the input distribution in the valence region and the corresponding gain in the sea region. There is a marked difference between  $P_{qq}$  and  $P_{gg}$  at lowest order and full order in the sea region. It originates from the fact that in the leading order kernels  $1/x$  terms are absent, while they are present at next-to-leading order. On the contrary, the other two kernels,  $P_{gq}$  and  $P_{gg}$ , have  $1/x$  terms both at leading order and next-to-leading order and the leading order contribution dominates. The above mentioned divergences of the kernels  $P_{gq}$  and  $P_{gg}$  for  $x \rightarrow 1$  are absent in  $P \otimes f_{\text{val}}$  due to the power behavior of  $f_{\text{val}}$  near 1.

The convolution of a valence-like function leads in the deep sea to a flat shape for all four kernels, as expected for  $1/x \otimes f_{\text{val}} \rightarrow \text{constant}$ . The plateau heights are characteristically different: smallest for  $P_{qq}$  and largest for  $P_{gg}$ .

### 5.2 Study of $f_{\text{sea}}(x) \rightarrow a(q) P(x, \alpha_s(q)) \otimes f_{\text{sea}}(x)$

Similarly, Fig. 6 shows the four convolutions of a *sea*-like distribution function chosen to be

$$f_{\text{sea}}(x) = 1.5 \log \left( 1 + \frac{0.04(1-x)}{x} \right).$$

It is similar to  $Q^+$  with regard to the behavior in the deep sea (see Fig. 7a). The asymptotic behavior in the deep sea is again determined by the  $1/x$  terms of the kernels with the effect that the linear logarithmic behavior turns into a quadratic one. The properties of the kernels generate a pattern analogous to the *valence*-like case. The  $P_{qq} \otimes f_{\text{sea}}$  becomes very small, while  $P_{gg} \otimes f_{\text{sea}}$  is strongly enhanced in the deep sea.

### 5.3 Some conclusions

The two opposite cases may serve to estimate the effect of a modification in the input distributions regarding the size and shape of the folded distributions. Three simple examples may illustrate it.

(a) Adding to the gluon function a small *valence*-like contribution would affect  $\partial_q Q^+$ , the slope of the singlet, in the deep sea by a small  $x$  independent upward shift. Figure 5b allows for a quantitative evaluation.

(b) Consider Fig. 1. Suppose a small *sea*-like contribution is added to the shape of the gluon distribution function, then Fig. 6b shows that to  $\partial_q Q^+$  in the deep sea would be added a term quadratic in  $\log 1/x$ , thus generating a non-trivial increase of the curvature of the singlet  $Q^+$ .

(c) It is also clear that a small modification of the  $x$  dependence of the singlet  $Q^+$  (for given  $q$ ) does not sizeably affect its slope in  $q$ .

It is interesting to note that all folded distributions are positive in the deep sea region regardless of whether they are

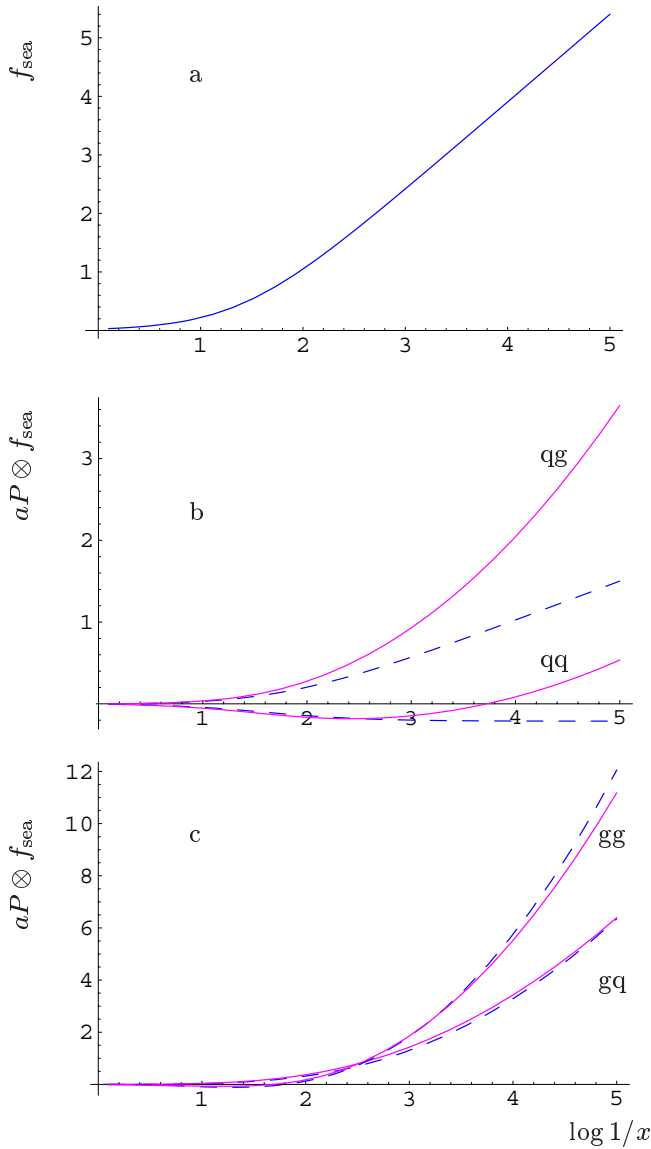


**Fig. 6.** Convolution of the sea-like distribution  $f_{\text{sea}}$  (uppermost curve) with the four kernels  $P_{ij}$  versus  $\log 1/x$ . Explanation of the curves as in caption of Fig. 5, exchanging *val* by *sea*

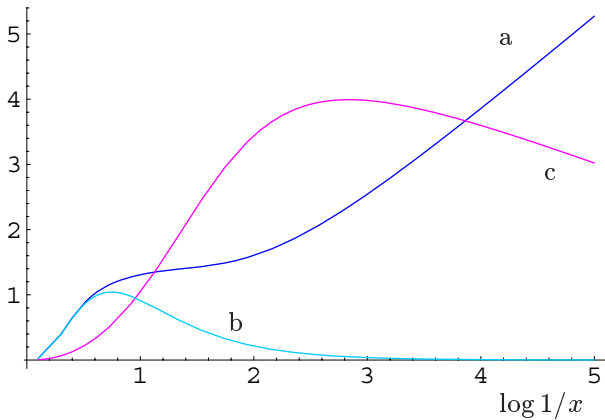


**Fig. 7.** The  $x$  distributions of  $Q^+(x, 1)$  **a**,  $Q^-(x, 1)$  **b** and the gluon  $G(x, 1)$  **c**

*valence-* or *sea-like*. This is different in the valence region. Therefore, compensating effects in the coupled DGLAP are possible in the valence region, but not so in the deep sea region.

Even if the distribution function  $f$  is independent of  $q$ , the folded distribution function  $P_{ij} \otimes f$  depends upon  $q$  through the  $\alpha_s$  dependence of the kernels  $P_{ij}$ .

## 6 The curvature

The first of the coupled DGLAP equations (see (4)), i.e.

$$\partial_q Q^+ = a(q) (P_{qq} \otimes Q^+ + P_{qg} \otimes G), \quad (5)$$

is differentiated with respect to  $q$  in order to obtain the required test quantity, yielding

$$\partial_q^2 Q^+(x, q) = (\text{Quark-term}) + (\text{Gluon-term}). \quad (6)$$

Each of the two terms consists in turn of three contributions.

The *Quark-term* is numerically small, because the  $q$  dependences of  $Q^+$  and of  $a(q)$  nearly compensate each other, as mentioned in Sect. 4. The numerical result is shown in Fig. 8 by curve d.

The *Gluon-term* with its three contributions is given explicitly in the following equation, (7):

$$\begin{aligned} \partial_q (a(q) P_{qg} \otimes G(x, q)) = & \\ & + \left( \frac{a'}{a} + \frac{\alpha_s'}{\alpha_s} \right) \cdot a(q) P_{qg} \otimes G \\ & - \frac{\alpha_s'}{\alpha_s} \cdot a(q) P_{qg}^{\text{LO}} \otimes G \\ & + a(q) P_{qg} \otimes \partial_q G. \end{aligned} \quad (7)$$

The prime ( $'$ ) in (7) denotes the derivative with respect to  $q$ . Equation (7) involves both the gluon distribution function  $G$  and its derivative  $\partial_q G$ . A closer inspection of the formula shows, however, that the dependence on the gluon is not strong. To this end it is noted that the expression

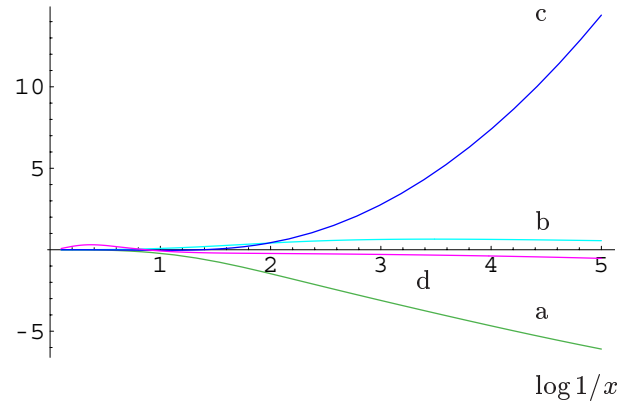


**Fig. 8.** Contributions to  $\partial_q^2 Q^+$  versus  $\log 1/x$  for  $q = 1$ . The curves represent the *Quark-term* **d** and the three contributions of the *Gluon-term*, i.e. term 1 **a**, term 2 **b** and term 3 **c**



$a(q) P_{qg} \otimes G$  follows directly from the first DGLAP equation (see (5)), namely

$$a(q) P_{qg} \otimes G = \partial_q Q^+ - a(q) P_{qq} \otimes Q^+. \quad (8)$$

It is determined by the experimental input distributions  $Q^+(x, 1)$  (see curve a in Fig. 7) and  $\partial_q Q^+(x, 1)$ . The gluon distribution function  $G(x, 1)$  itself can be obtained from the constraint equation (8). Given the properties of the kernel  $P_{qg}$  the magnitude and shape of  $G(x, 1)$  are defined and little scope for variations is left. Figure 7 (curve c) shows the resulting distribution.

The three terms of (7) are discussed one by one and evaluated for  $q = 1$ .

- *Term 1*: The  $x$  dependence is given by (8), since the factor  $a'/a + \alpha'_s/\alpha_s$  is independent of  $x$  and, for  $q = 1$ , equals  $-1.3$ .
- *Term 2* involves the gluon folded with the leading order kernel  $P_{qg}^{LO}$ , which has the simple form  $x^2 + (1-x)^2$ ; it is numerically insignificant.
- *Term 3* involves  $\partial_q G$  and is the critical one. The expression for  $\partial_q G$  is given by the second of the coupled DGLAP equations (see (4)):

$$\partial_q G = a(q) (P_{qg} \otimes Q^+ + P_{gg} \otimes G). \quad (9)$$

Insertion in term 3 yields

$$\begin{aligned} a(q) P_{qg} \otimes \partial_q G \\ = a(q) P_{qg} \otimes G \cdot a(q) \frac{P_{qg} \otimes (P_{qg} \otimes Q^+ + P_{gg} \otimes G)}{P_{qg} \otimes G}. \end{aligned}$$

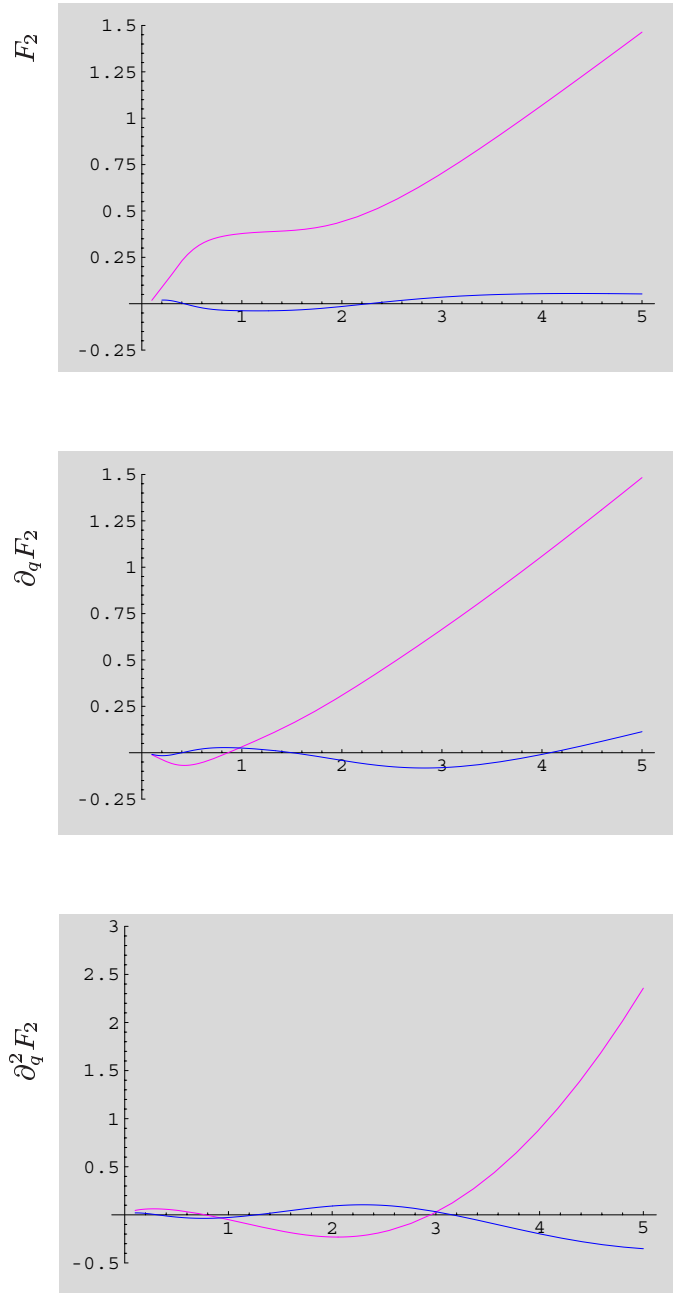
The first factor (see (8)) does not depend upon the gluon, while in the second factor, the ratio, the gluon appears both in the numerator and the denominator. Its magnitude cancels and its shape affects the ratio only weakly. In the deep sea the ratio is well approximated by

$$1.2 a \frac{P_{qg} \otimes P_{gg}^{LO} \otimes G}{P_{qg} \otimes G}.$$

Recalling the structure of the kernels it is quite evident that the numerator is sensitive to  $\frac{1}{x} \otimes \frac{1}{x}$ , while the denominator is sensitive only to one  $\frac{1}{x}$ -operator. It is then not so surprising that term 3 with  $\partial_q G$  dominates the behavior in the deep sea and unavoidably produces a strong  $x$  dependence.

The quantitative evaluation of the contributions to the curvature is carried out using the singlet and gluon distribution functions displayed in Fig. 7. The results are shown in Fig. 8. The contribution of the *Quark-term* (curve d) is negative and very close to 0, as anticipated. The three contributions from the *Gluon-term* decrease linearly (a), remain approximately constant (b) and increase quadratically (c).

It is concluded that  $Q^+(x, q)$  has a significant positive curvature in the deep sea region, where the contribution from  $\partial_q G$  outnumbers all other contributions. The  $x$  behavior of the curvature is a *property of the kernels* and is hardly sensitive to the size and shape of the gluon. The quantity  $\partial_q^2 Q^+(x, q)$  probes in a non-trivial way both DGLAP equations and their kernels.



log 1/x

**Fig. 9.** Effect of the coefficient functions to  $N + \epsilon Q^+$  and its derivatives versus  $\log 1/x$  for  $q = 1$

### 7 Prediction of $\partial_q^2 F_2^{ep}$

The theoretical expression for  $F_2^{ep}$  is given in (2). It involves the parton distributions and the coefficient functions  $C_F$  and  $C_G$ . The quantity to be determined is the second derivative of  $F_2^{ep}$  with respect to  $q$ , i.e.

$$\partial_q^2 F_2^{ep} = \partial_q^2 (C_F \otimes (N + \epsilon Q^+) + C_G \otimes \epsilon G),$$

evaluated in the deep sea and for  $q = 1$ . In addition to the dominating contribution of  $\partial_q^2 Q^+$  discussed in Sect. 7,

also the effect of the non-singlet  $N$  and the coefficient functions together with their respective derivatives have to be considered.

$C_F$ , the first coefficient function, consists of two distributions, a  $\delta$  distribution, which reproduces  $N + \epsilon Q^+$ , and a *plus*-distribution applied to  $N + \epsilon Q^+$  contributing at order  $\alpha_s/2\pi$ .

$N + \epsilon Q^+$  is dominated by the singlet  $Q^+$ . Even in the deep sea the non-singlet  $N$  is not vanishing, since at  $Q^2 = 4.5 \text{ GeV}^2$  the charmed sea is not yet fully developed, implying  $\bar{c} - \bar{s} < 0$ . However, the evolution of the non-singlet contributes negligibly to the first and second derivative of  $F_2^{ep}$ .

The gluon and its derivatives with respect to  $q$  contribute directly through the second coefficient function  $C_G$  and also in the evaluation of  $\partial_q^2 Q^+$ .

Figure 9 shows the contribution arising from the coefficient functions to  $N + \epsilon Q^+$  and its derivatives. As anticipated,  $N + \epsilon Q^+$  is a good approximation to  $F_2^{ep}$  and as well for the first derivative with respect to  $q$ . The second derivative is modified in the deep sea regime by less than about 10%. The contribution of the non-singlet to  $\partial_q^2 F_2$  is negligible.

In conclusion: the statement that  $\partial^2 Q^+$  is significantly positive remains valid also for  $\partial^2 F_2^{ep}$ . This conclusion is stable against variations of the input distributions.

It may be noted that, qualitatively, the feature of a positive curvature can be deduced already from the theoretical study [14] predicting an unbounded growth of  $F_2$  with  $1/x$  under certain uniformity assumptions.

## 8 Conclusions

A dedicated investigation of the DGLAP kernels in the low- $x$  regime has been performed. Their striking feature is the presence of  $1/x$  terms producing a strong rise in  $F_2$  for  $x < 0.001$ . Previous QCD analyses based on low energy lepton–nucleon data did not probe that behavior, since they reached hardly below  $x = 0.01$ . Recent global QCD analyses, which also include the low- $x$  HERA  $F_2$  data, are only partially sensitive to the low- $x$  behavior of the kernels, because the relevant data represent a small fraction of the data entering the global fit and thus their effect to the overall  $\chi^2$  remained unnoticed.

The study presented here was focused directly on the deep sea and has examined the second derivative of the structure function  $F_2^{ep}$  with respect to  $q$  as a quantity for probing the low- $x$  feature of the DGLAP kernels. The main result is shown in Fig. 10. The DGLAP kernels predict a significant positive curvature of  $F_2$  at fixed  $q = 1$  in the low- $x$  region in contrast to the flat behavior in  $q$  of the HERA  $F_2$ -data. The deviation increases with decreasing  $x$ . This conclusion is stable against changes of the shape of the parton distribution functions, in particular of the gluon distribution.

It is interesting to note that  $P_{ij} \otimes f$  is positive for all kernels provided  $x$  is deep enough in the sea region and  $f$  positive definite. This implies for the DGLAP equations

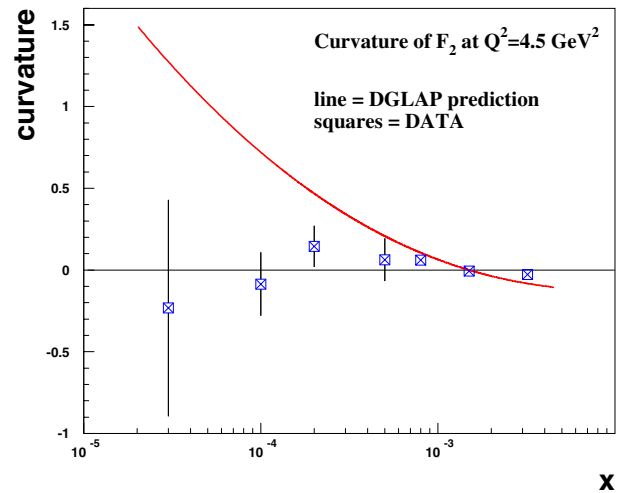


**Fig. 10.** Measured and calculated curvature of  $F_2$  for  $q = 1$  versus  $x$

that in the deep sea the derivatives of the singlet and the gluon receive positive contributions from both the folded singlet and the folded gluon, contrary to mutual compensations possible in the valence region.

*Acknowledgements.* I like to thank J. Bartels, T. Gehrmann, H. Spiesberger and P.M. Zerwas for valuable discussions.

## References

1. T. Eichten et al., Phys. Lett. B **46**, 274 (1973)
2. P.M. Zerwas, H.A. Kastrup, QCD – 20 years later (World Scientific, Singapore 1993), 1–867
3. V.N. Gribov, L.N. Lipatov, Yad. Fiz. **15**, 781 (1972); Sov. J. Nucl. Phys. **15**, 438 (1972)
4. G. Altarelli, G. Parisi, Nucl. Phys. B **126**, 298 (1977)
5. C. Adloff et al., Nucl. Phys. B **497**, 3 (1997); S. Aid et al., Nucl. Phys. B **470**, 3 (1996); T. Ahmed et al., Nucl. Phys. B **439**, 471 (1995); C. Adloff et al., Eur. Phys. J. C **30**, 1 (2003)
6. J. Breitweg et al., Phys. Lett. B **487**, 53 (2000); J. Breitweg et al., Phys. Lett. B **407**, 432 (1997); M. Derrick et al., Z. Phys. C **69**, 607 (1996); J. Breitweg et al., Eur. Phys. J. C **7**, 609 (1999); S. Chekanov et al., Eur. Phys. J. C **21**, 443 (2001)
7. A.D. Martin et al., Eur. Phys. J. C **23**, 73 (2002)
8. J. Pumplin et al., hep-ph/0201195 (2002)
9. M. Glück, E. Reya, A. Vogt, Eur. Phys. J. C **5**, 461 (1998)
10. D. Haidt, DIS96, Rome, April 1996 (World Scientific Publishing, 1997), 179
11. W. Buchmüller, D. Haidt, Double Logarithmic Scaling of the Structure Function  $F_2$  at Small  $x$ , hep-ph/9605428
12. D. Haidt, DIS97, Chicago, April 1997, AIP Conference Proceedings **407**, 386 (1997)
13. W. Furmanski, R. Petronzio, Z. Phys. C **11**, 293 (1982)
14. A. De Rujula et al., Phys. Rev. D **10**, 1649 (1974)